Variability of the gravitationally lensed blazar PKS 1830-211

Sarah Maria Wagner-Hall

Image: https://www.esa.int/ESA_Multimedia/Images/2015/07/Gravitational_lensing#.YzTN2pCFR7g.link

Research Interests?

Simulating particle acceleration with stochastic differential equations

$$\frac{dX_{t,i}}{dt} = A_i(t, \boldsymbol{X}_t) + \sum_{j=1}^{N} B_{ij}(t, \boldsymbol{X}_t)\frac{dW_{t,j}}{dt}$$

$$\frac{\partial f(t,\boldsymbol{x})}{\partial t} = -\sum_{i=1}^{N}\frac{\partial}{\partial x_i}\left(A_i(t,\boldsymbol{x})f(t,\boldsymbol{x})\right) + \\ + \frac{1}{2}\sum_{i=1}^{N}\sum_{j=1}^{N}\frac{\partial^2}{\partial x_i \partial x_j}\left(\sum_{k=1}^{N} B_{ik}(t,\boldsymbol{x})B^{\mathrm{T}}_{kj}(t,\boldsymbol{x})f(t,\boldsymbol{x})\right)$$

Research Interests?

Simulating particle acceleration with stochastic differential equations

$$\frac{dX_{t,i}}{dt} = A_i(t, \boldsymbol{X}_t) + \sum_{j=1}^{N} B_{ij}(t, \boldsymbol{X}_t)\frac{dW_{t,j}}{dt}$$

$$\frac{\partial f(t,\boldsymbol{x})}{\partial t} = -\sum_{i=1}^{N}\frac{\partial}{\partial x_i}\left(A_i(t,\boldsymbol{x})f(t,\boldsymbol{x})\right) + \\ + \frac{1}{2}\sum_{i=1}^{N}\sum_{j=1}^{N}\frac{\partial^2}{\partial x_i \partial x_j}\left(\sum_{k=1}^{N} B_{ik}(t,\boldsymbol{x})B^{\mathrm{T}}_{kj}(t,\boldsymbol{x})f(t,\boldsymbol{x})\right)$$

Research Interests?

Simulating particle acceleration with stochastic differential equations

$$\frac{dX_{t,i}}{dt} = A_i(t, \boldsymbol{X}_t) + \sum_{j=1}^{N} B_{ij}(t, \boldsymbol{X}_t)\frac{dW_{t,j}}{dt}$$

$$\frac{\partial f(t,\boldsymbol{x})}{\partial t} = -\sum_{i=1}^{N}\frac{\partial}{\partial x_i}\left(A_i(t,\boldsymbol{x})f(t,\boldsymbol{x})\right) + \\ + \frac{1}{2}\sum_{i=1}^{N}\sum_{j=1}^{N}\frac{\partial^2}{\partial x_i \partial x_j}\left(\sum_{k=1}^{N} B_{ik}(t,\boldsymbol{x})B_{kj}^{\mathrm{T}}(t,\boldsymbol{x})f(t,\boldsymbol{x})\right)$$

Time series analysis of blazar light curves

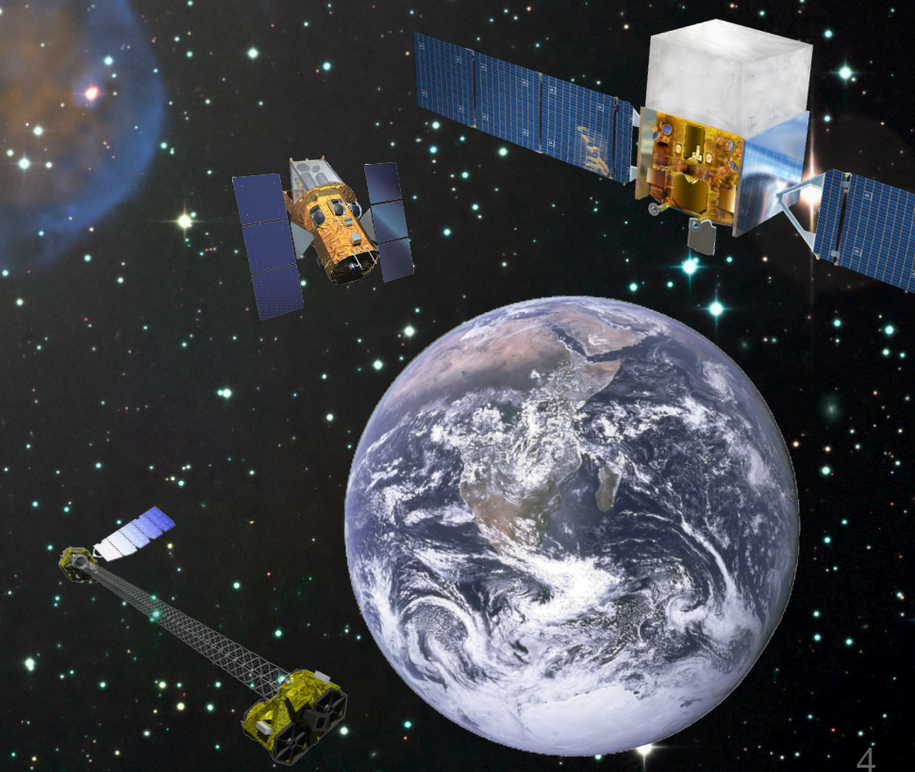

Research Interests?

Simulating particle acceleration with stochastic differential equations

$$\frac{dX_{t,i}}{dt} = A_i(t, \boldsymbol{X}_t) + \sum_{j=1}^{N} B_{ij}(t, \boldsymbol{X}_t)\frac{dW_{t,j}}{dt}$$

$$\frac{\partial f(t,\boldsymbol{x})}{\partial t} = -\sum_{i=1}^{N}\frac{\partial}{\partial x_i}\left(A_i(t,\boldsymbol{x})f(t,\boldsymbol{x})\right) + \\ + \frac{1}{2}\sum_{i=1}^{N}\sum_{j=1}^{N}\frac{\partial^2}{\partial x_i \partial x_j}\left(\sum_{k=1}^{N} B_{ik}(t,\boldsymbol{x})B^{\mathrm{T}}_{kj}(t,\boldsymbol{x})f(t,\boldsymbol{x})\right)$$

Time series analysis of blazar light curves

Variability of the gravitationally lensed blazar PKS 1830-211

Sarah Maria Wagner-Hall

Image: https://www.esa.int/ESA_Multimedia/Images/2015/07/Gravitational_lensing#.YzTN2pCFR7g.link

PKS 1830-211

blazar (FSRQ)

gravitationally lensed

close to galactic plane

two images within ~1 arcsec

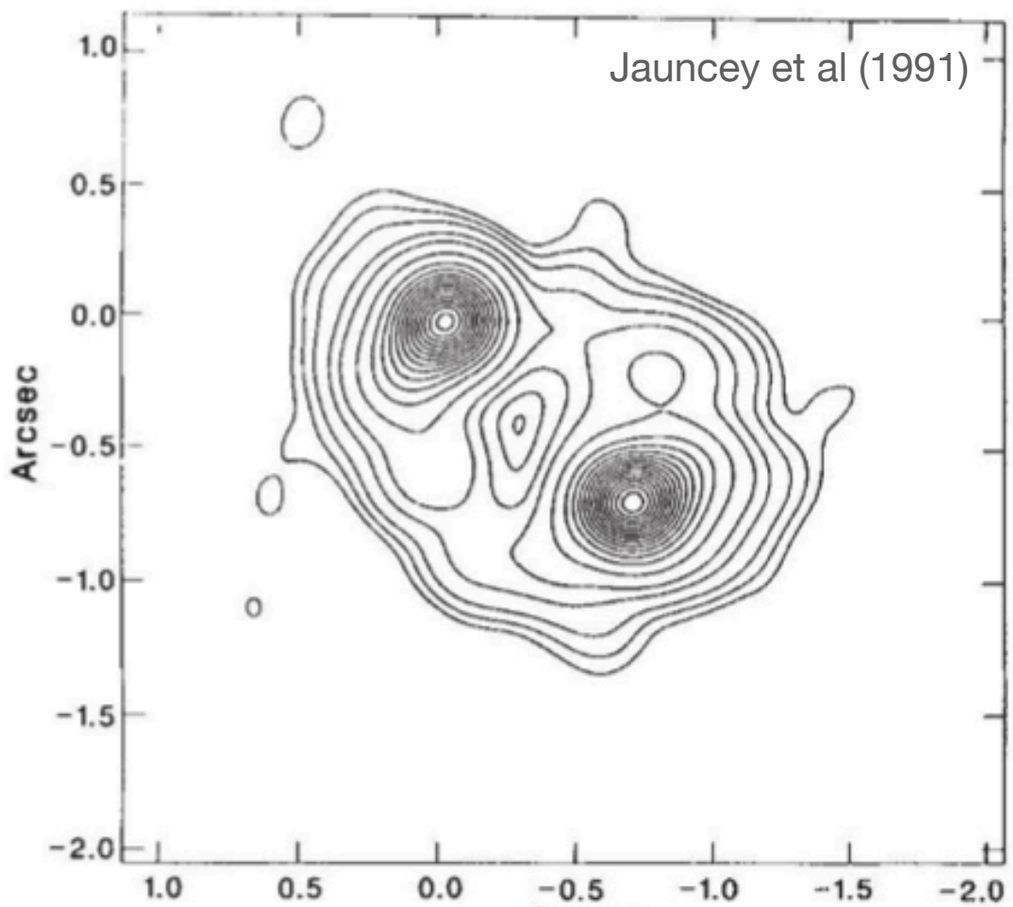

FIG. 1 The MERLIN 1.692-GHz hybrid map of PKS1830−211 shown as both a contour map and in relief. The restoring beam is a circular gaussian with a full width at half maximum (FWHM) of 0.25". Contour levels are at −0.005, 0.005, 0.01, 0.02, 0.05, 0.1, 0.25, 0.5, 0.75, 1.0, 1.25, 1.5, 1.75, 2.0, 2.25, 2.5, 2.75, 3.0, 3.25 and 3.5 Jy per beam. The relief image plots the square root of the amplitude to emphasize the presence of the ring-like structure.

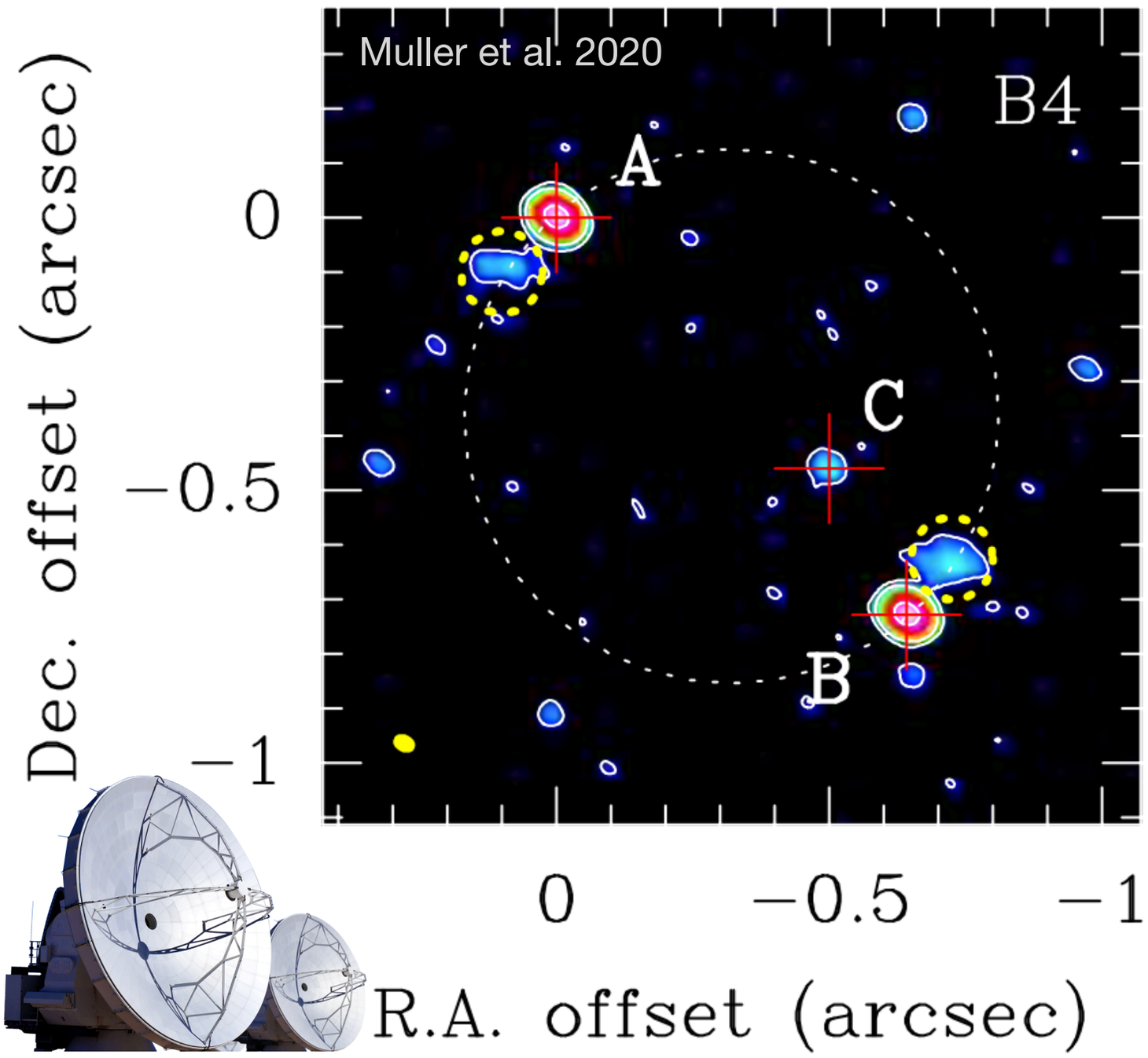

weak third image detected with ALMA

resolved with Chandra

Available Data

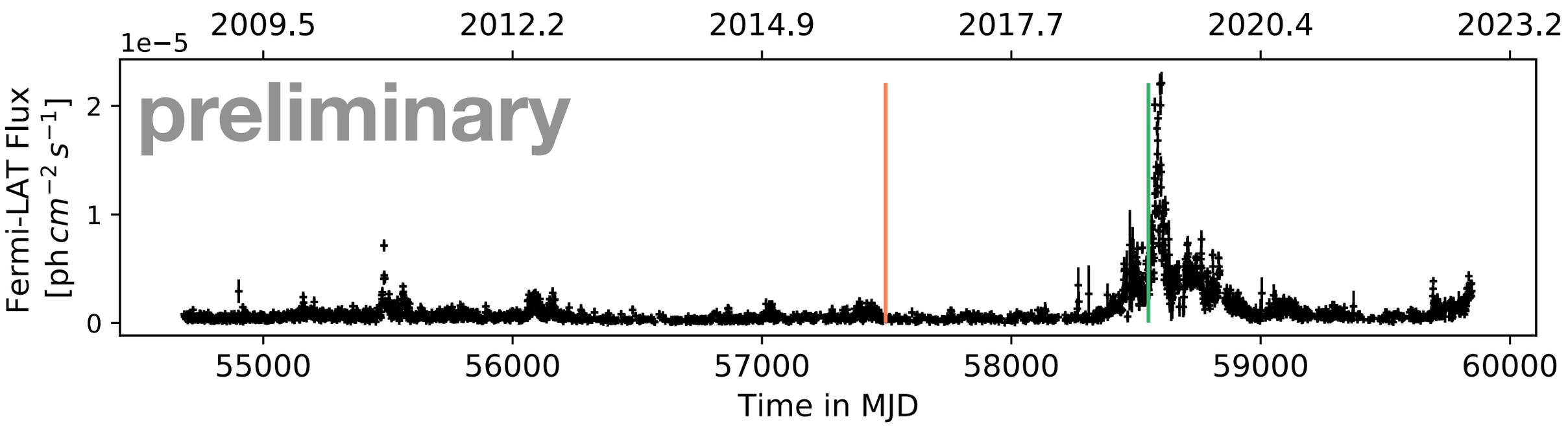

Available Data

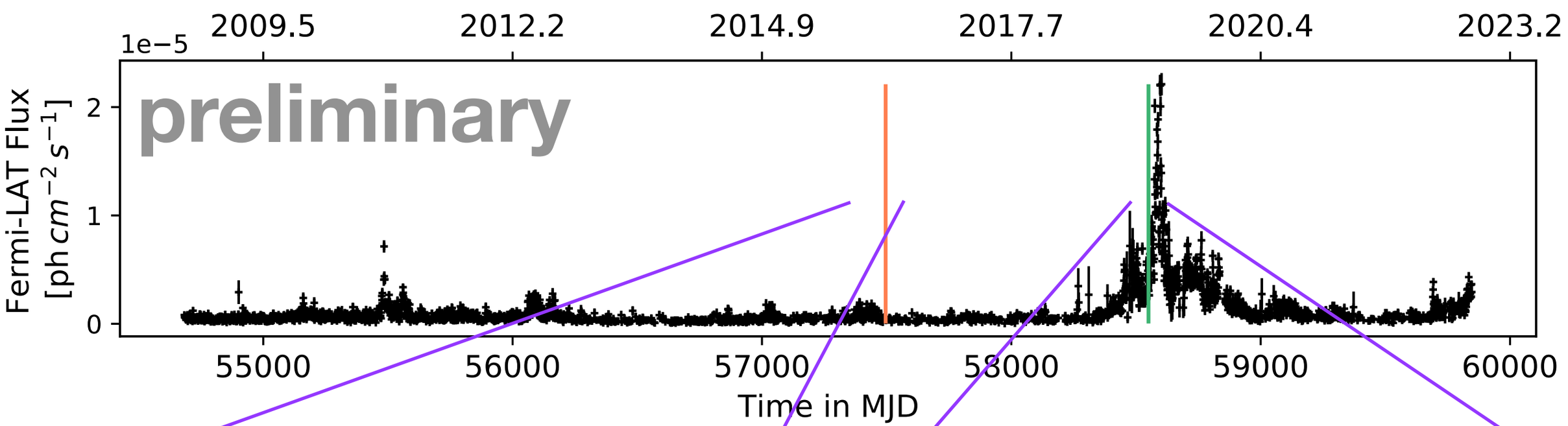

2016

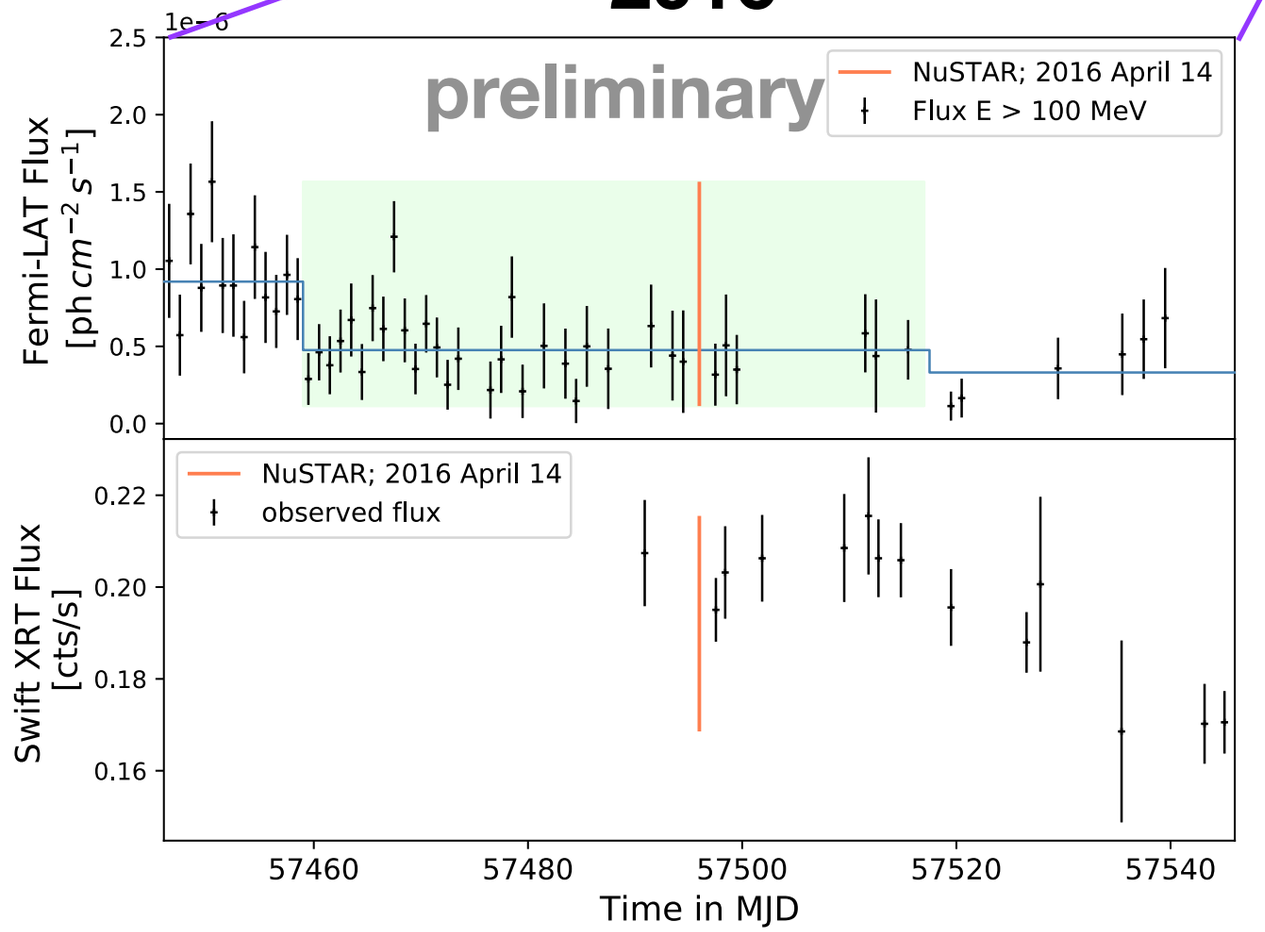

2019

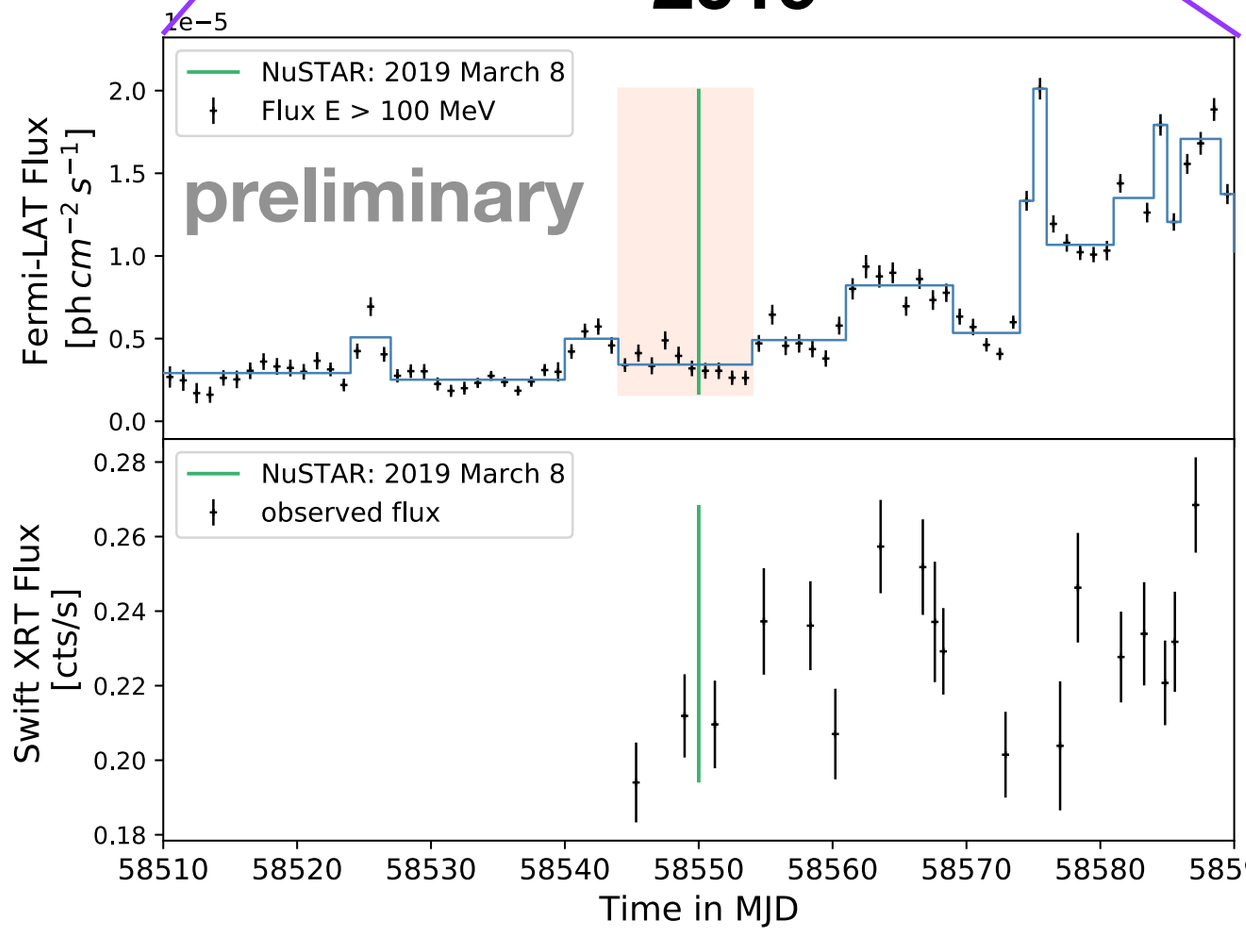

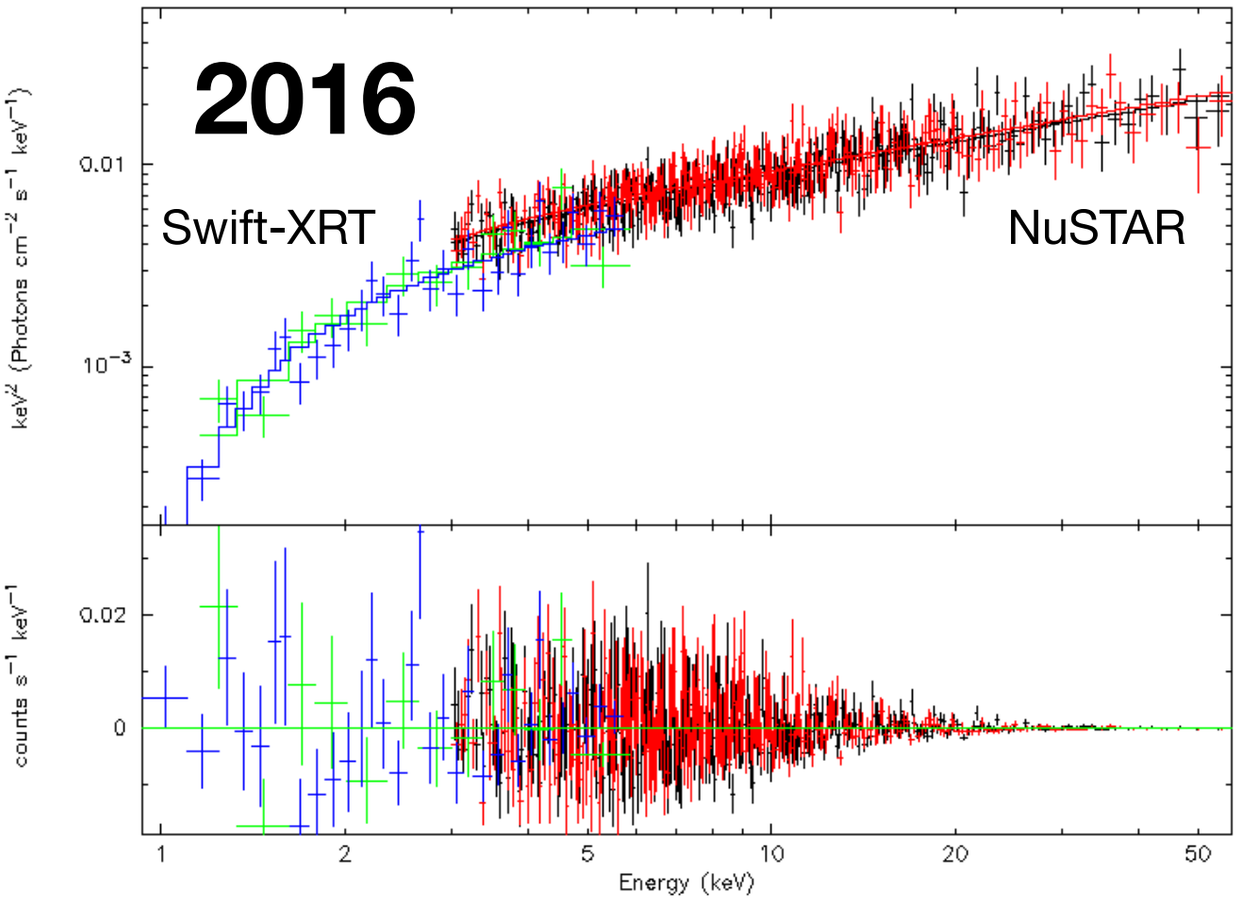

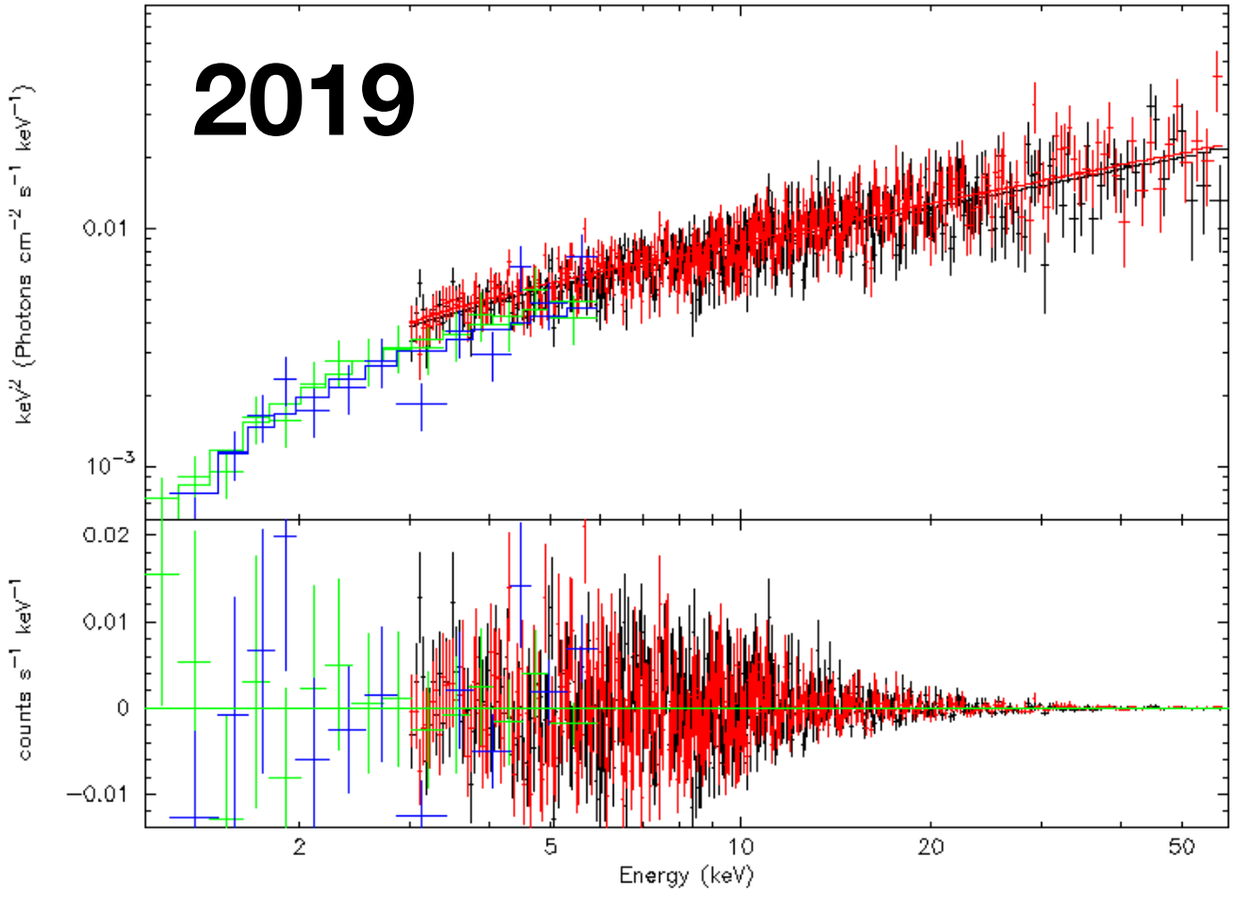

X-ray Spectral Analysis

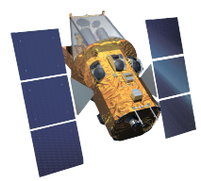

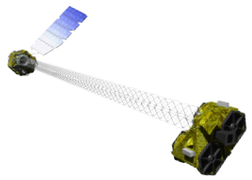

- Systematically smaller power-law indices for independent Swift XRT analysis
- Swift XRT data is heavily absorbed!
- NuSTAR data is crucial to determine underlying continuum
- Joint analysis to adequately fit spectral properties:
  power-law index ~ 1.4

Gamma-ray Spectral Analysis

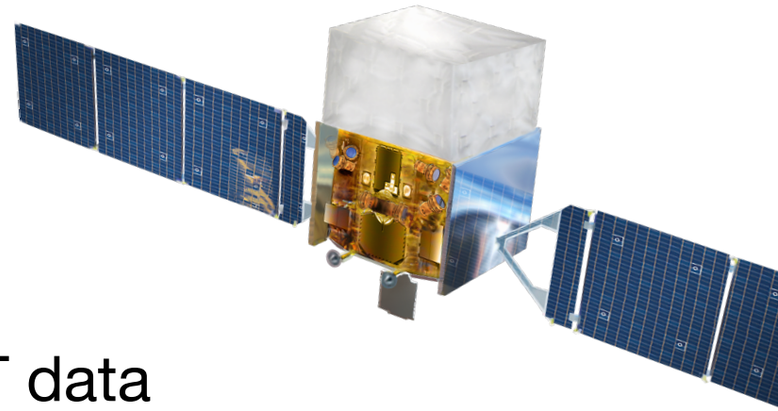

Fermi-LAT data

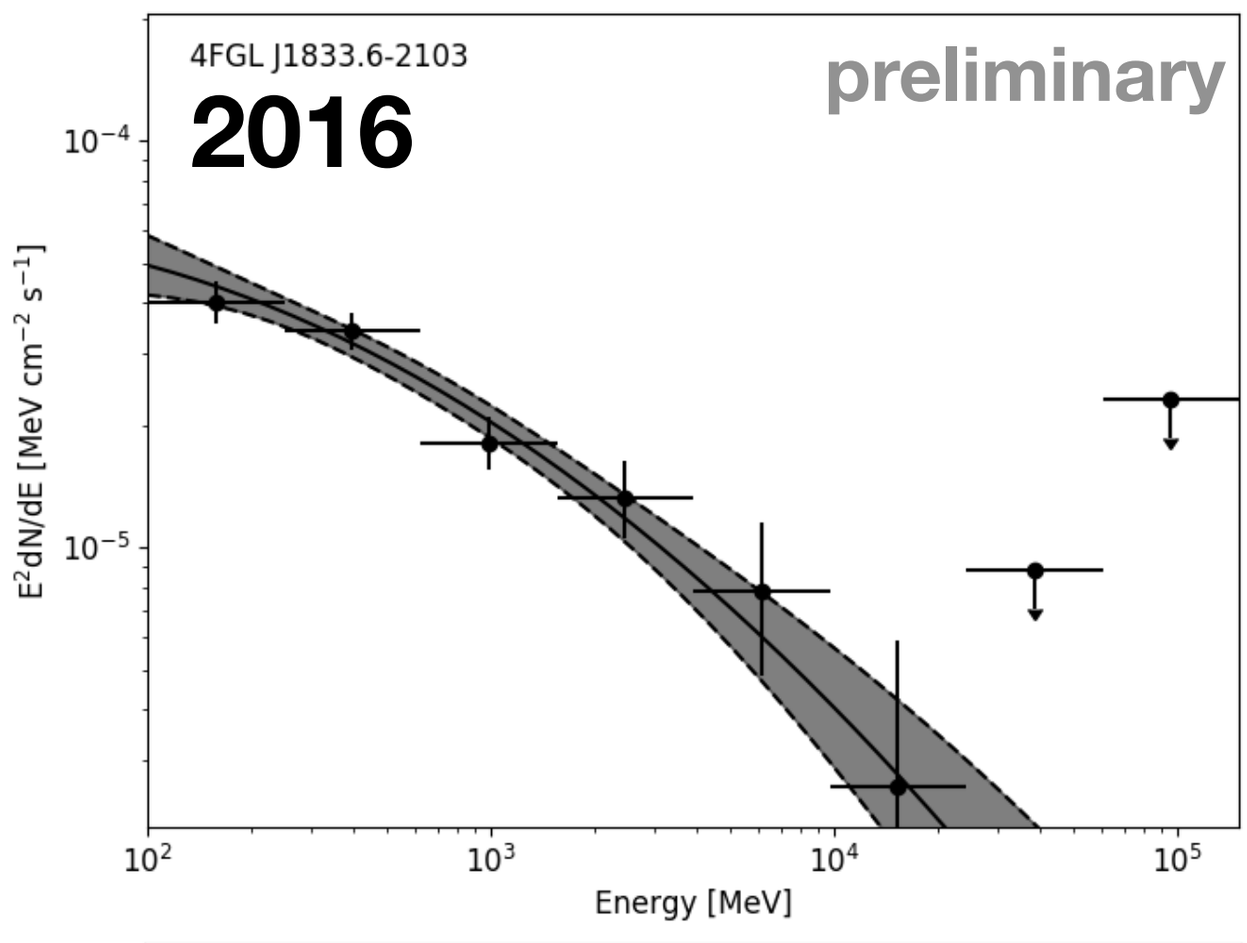

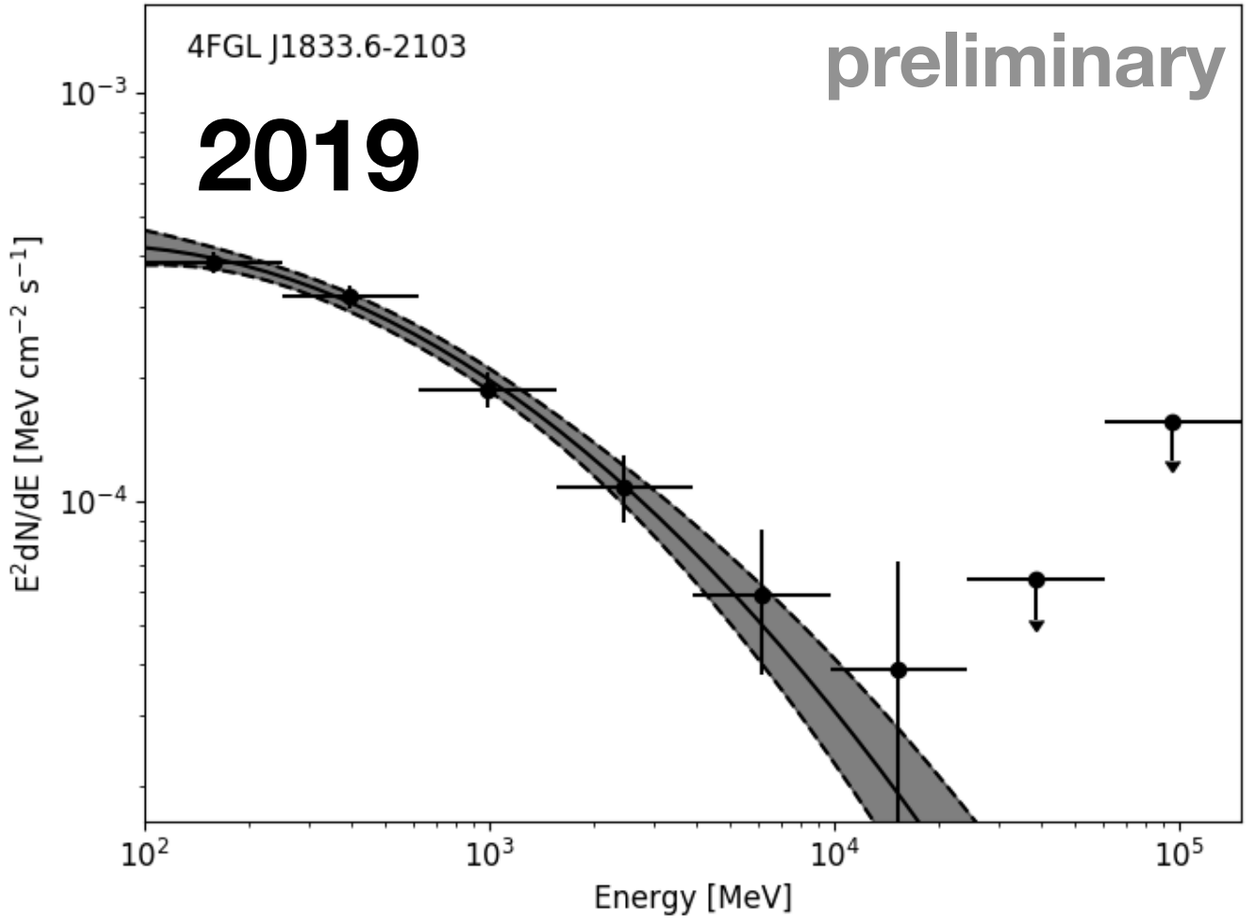

- Note order of magnitude difference on y-axis
- amplitude of gamma-ray variability appears much larger than x-ray variability

Multi-wavelength SED modeling

- non-thermal leptonic emission (BLAZAR, Moderski et al. 2013)
- spherical emission zone moving along conical jet
- inject energetic particles following a broken power-law distribution
- integrate emission (SYN, SSC, ERC_BLR, ERC_DT) over injection distance

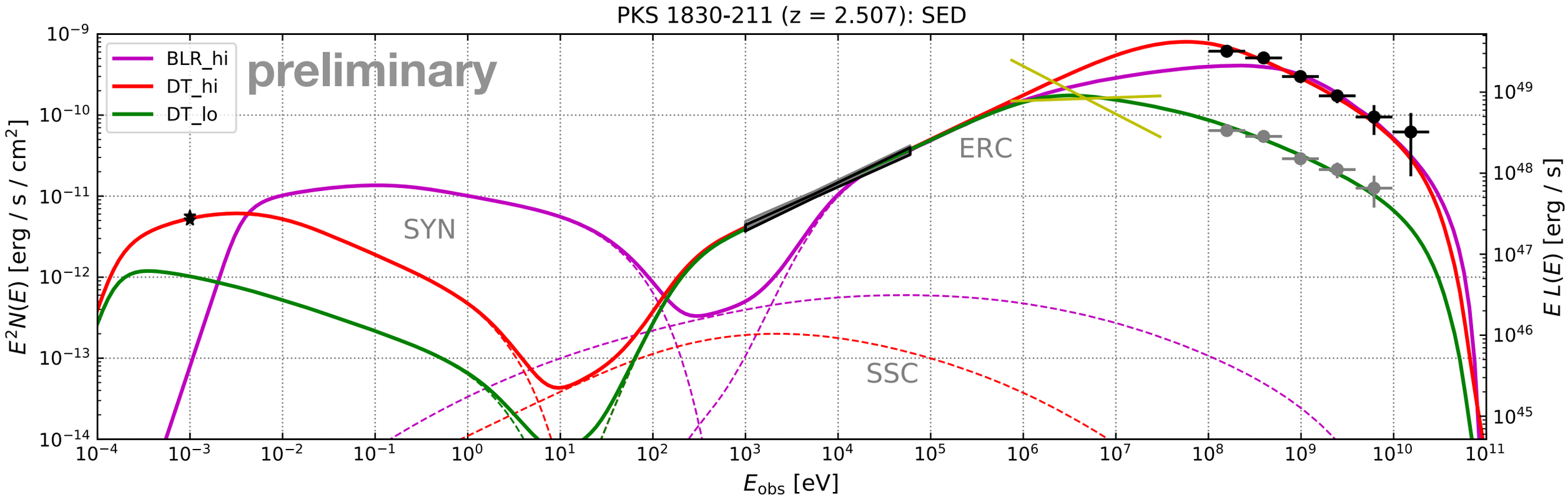

Multi-wavelength SED modeling

- significant SSC contribution is incompatible with differing amplitudes
- focus on single ERC component (typical for FSRQ) with two distance scales:
  - r_BLR (magenta): cannot reproduce soft x-ray and gamma-rays
  - r_DT_hi (red): fits the high state data well
  - r_DT_lo (green): fits the low state data well (lower break in el distribution)

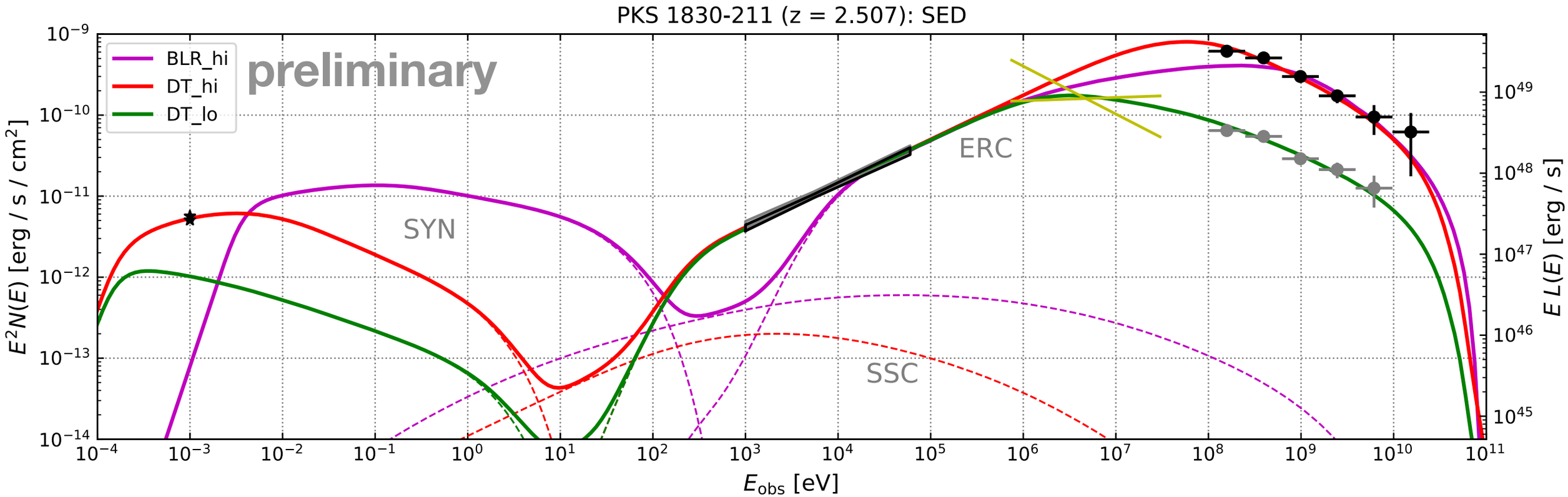

Analysis of time delay

If the tow lensed images are not resolved, the light curve should be a superposition of the source intrinsic light curve and a delayed, magnified version of itself.

Auto-correlation

$$R_y(\tau) = E\left[y(t)\, y(t-\tau)\right]$$

- Auto-correlation theorem (Fourier Transform)
- Double Power Spectrum (Barnacka et al. 2011)
- Discrete Correlation Function (Edelson & Krolik 1988)
- Structure function
- …

Model fitting

$$y(t) = x(t) + a\, x(t-\tau)$$

- utilize fact that we expect to know the behavior of the light curve based on the gravitational lensing

Discrete Correlation Function

$$UDCF_{i,j} = \frac{(a_i - \bar{a})\,(b_j - \bar{b})}{\sqrt{(\sigma_a^2 - e_a^2)\,(\sigma_b^2 - e_b^2)}}$$

detrend per bin

normalize

Auto-correlation of PKS 1830-211 with LC-binning: 1day

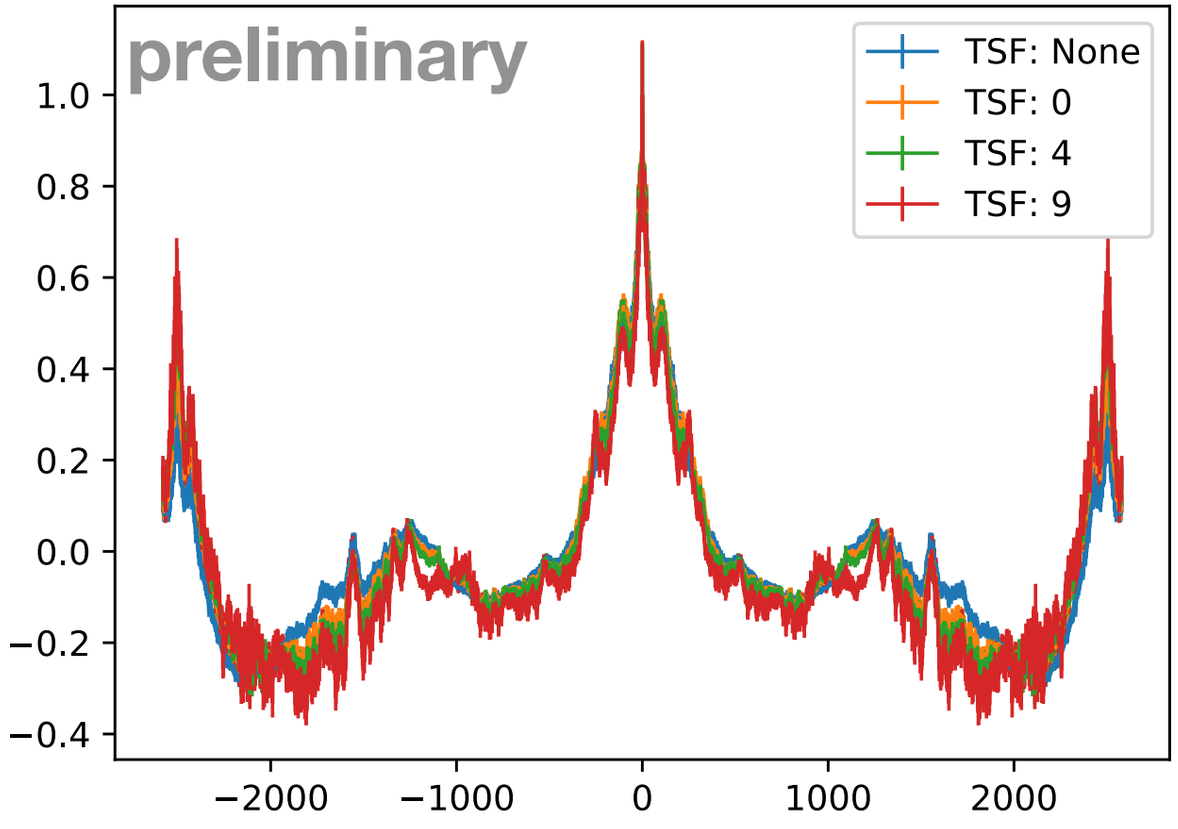

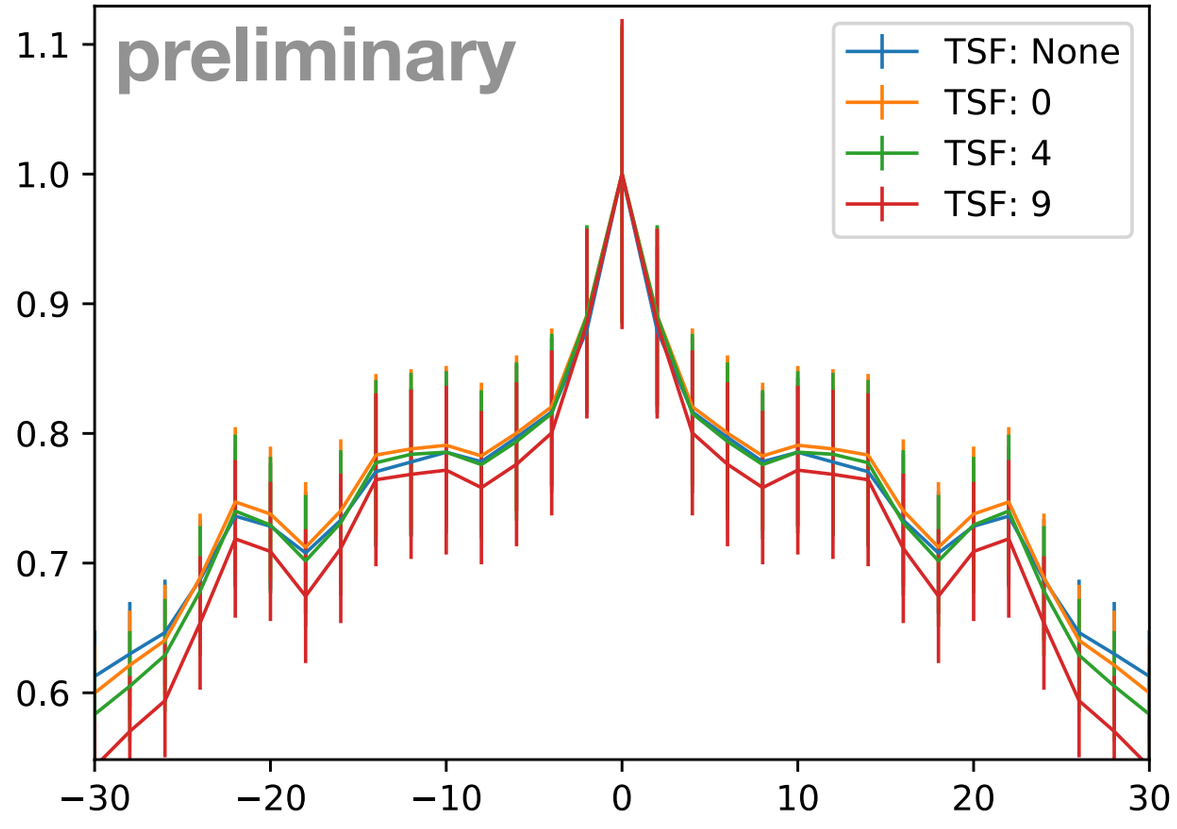

Edelson & Krolik 1988

Fourier Transform (LSP)

The auto-correlation corresponds to the FT of the (Lomb-Scargle) Periodogram:

$$R(x) = \int_{-\infty}^{+\infty} f(u) f^*(u-x) du = \int_{-\infty}^{+\infty} |F_{LS}(s)|^2 e^{i2\pi sx} ds$$

ACF through LSP, PKS 1830-211, 1d binning

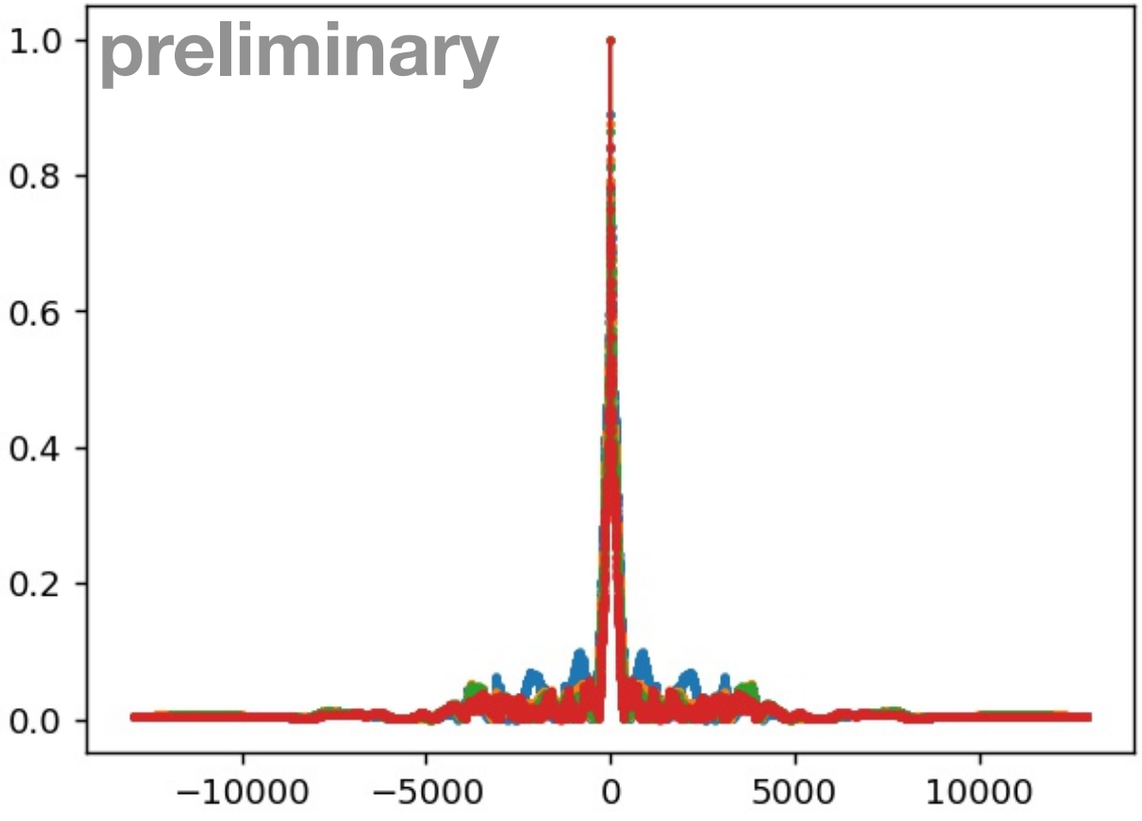

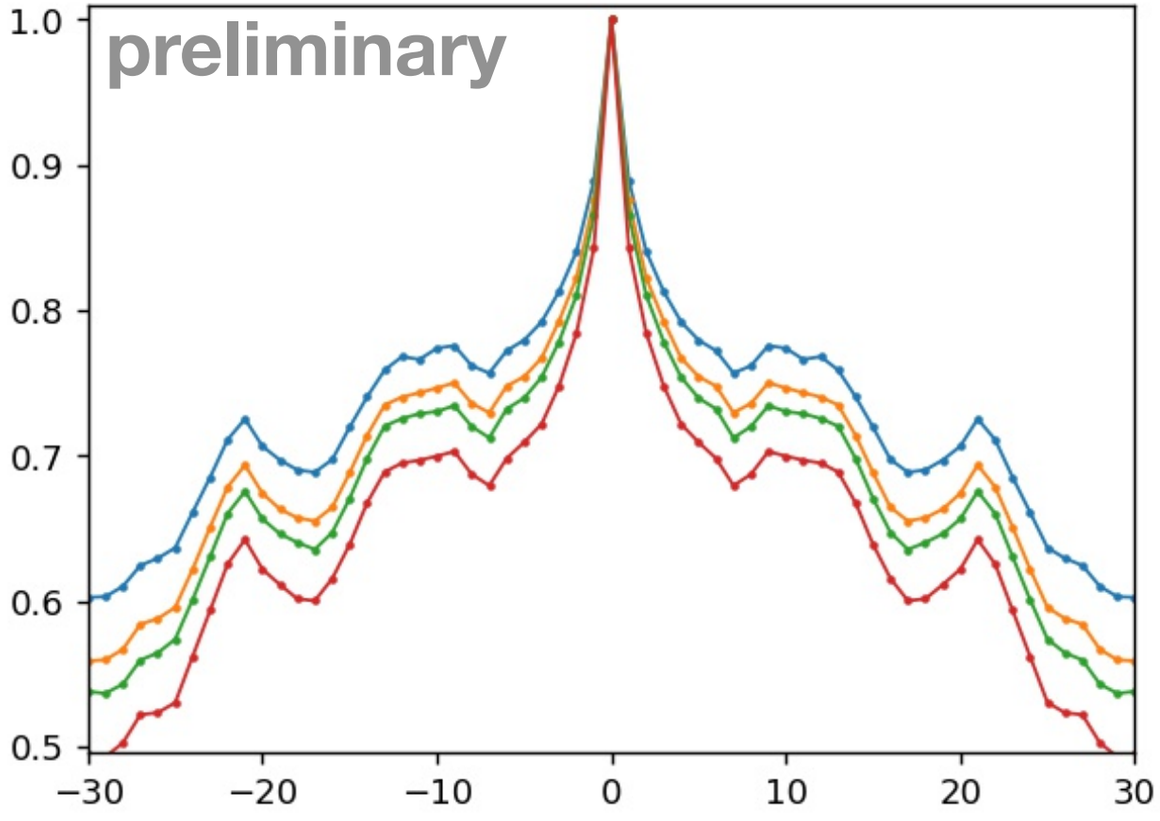

The lightcurves package

swagner-astro / lightcurves Public

A package to analyze any kind of light curve/time serie
Bayesian Blocks, flare fitting (HOP), and a stochastic p

2 stars 4 forks

Star Un

Code Issues Actions

Search projects

lightcurves 0.0.5

```
pip install lightcurves
```

Latest version

Released: Jun 8, 2022

Summary & Outlook

- PKS 1830-211 shows high and low gamma-ray activity at comparable states of x-ray activity (modeled with EC from DT)

- Compare traditional ACF methods to new model fitting approach

- Check significance with mock light curves (e.g. different colored noise as in Barnacka et al. 2015)

- Time-tagged photon analysis of NuSTAR data

Thank you!

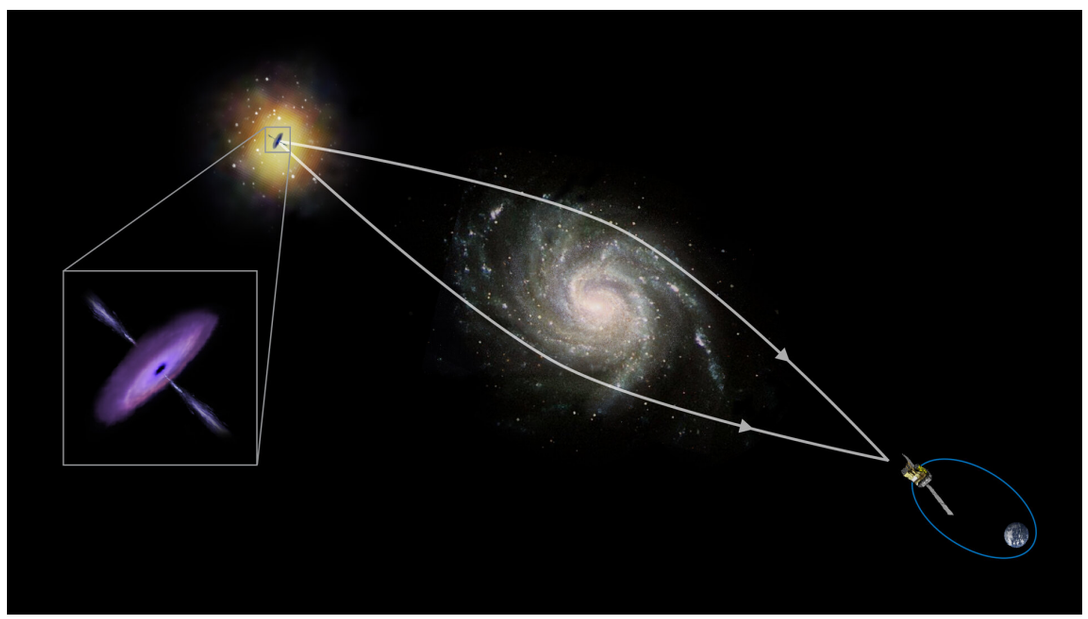

Backups

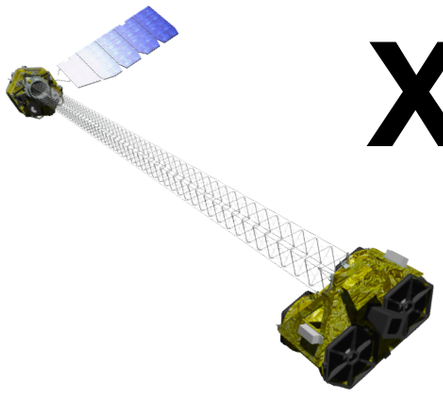

X-ray Spectral Analysis

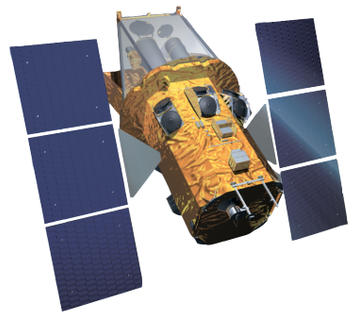

Simultaneous fitting of:

NuSTAR FPMA + NuSTAR FPMB + Swift XRT (before) + Swift XRT (after)

with

1) absorbed power-law: tbabs * powerlaw

2) double absorbed power-law: ztbabs * tbabs * powerlaw

3) absorbed log-parabola: tbabs * logpar

and

- n_H either free or fixed to Galactic value: n_H = 0.18e22
- normalization free to vary (calibration between instruments)
- for tbabs: z_lens = 0.88

Gamma-ray Spectral Analysis

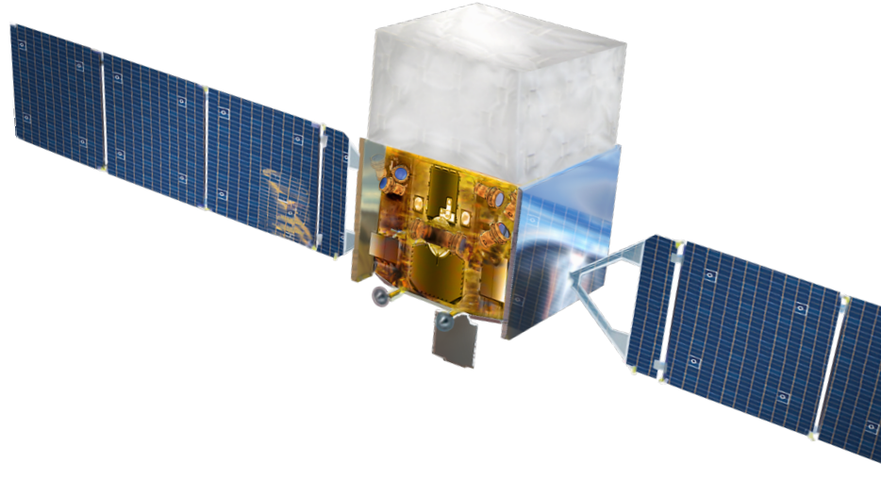

Standard Analysis for spectra:

- Fermitools 1.2.23 & fermipy 0.20.0
- Energy range: 100 MeV – 300 GeV
- Zmax: 90
- Event class: 128
- Event type: 3
- Filter: DATA_QUAL > 0 & LAT_CONFIG == 1
- T in MET: 479433604 – 484444804 (2016);
- 573177605 – 574041605 (2019)
- ROI: 10 deg
- Galactic diffusion: gll_iem_v07.fits
- Isotropic diffusion: iso_P8_R3_SOURCE_V2_v1.txt
- Catalog: gll_psc_v26.xml

analogously for light curves over the full observation period

X-ray Variability (NuSTAR)

New method: unbinned, time-tagged photon Bayesian block analysis

consider individual observation runs with several GTIs (one bin)

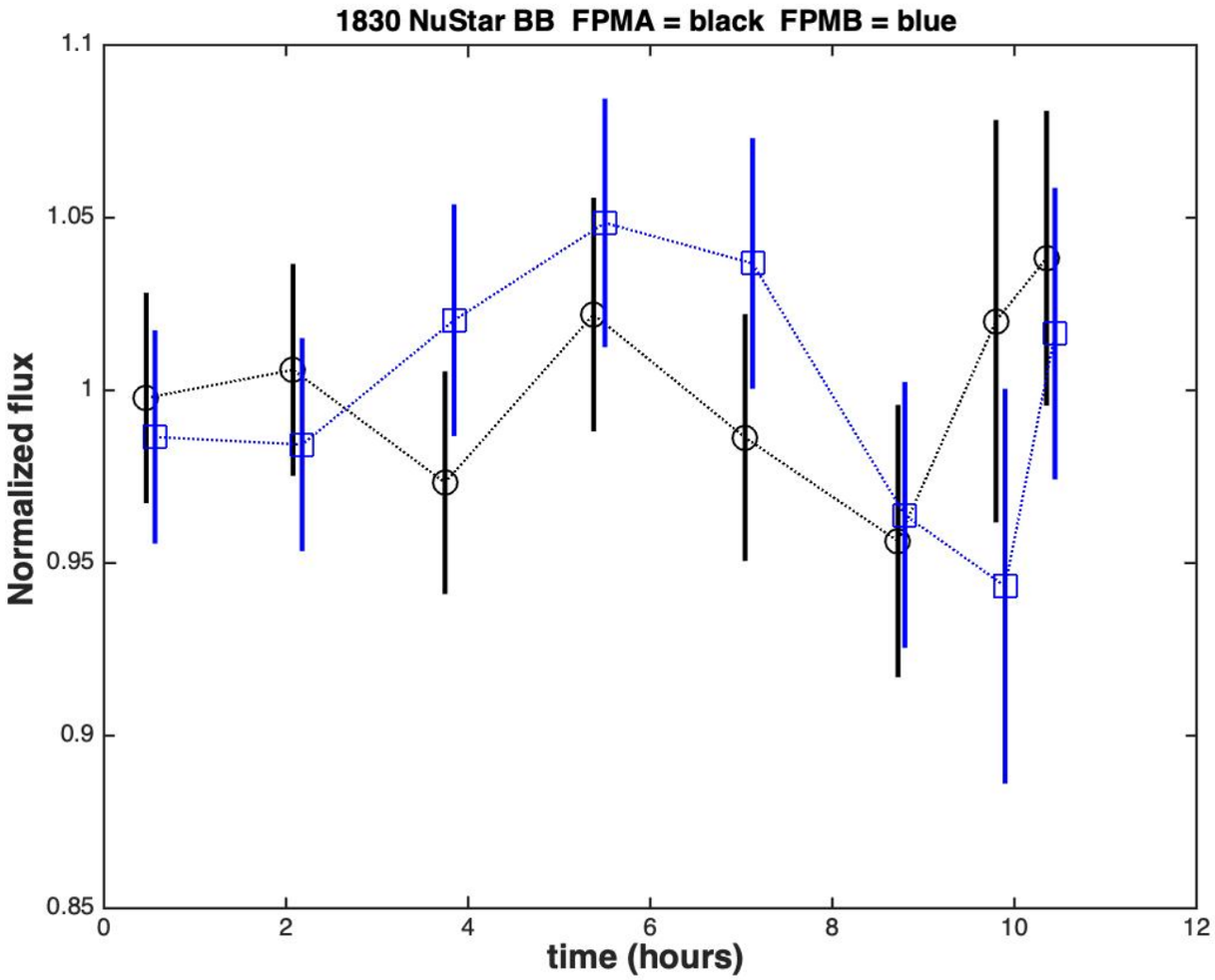

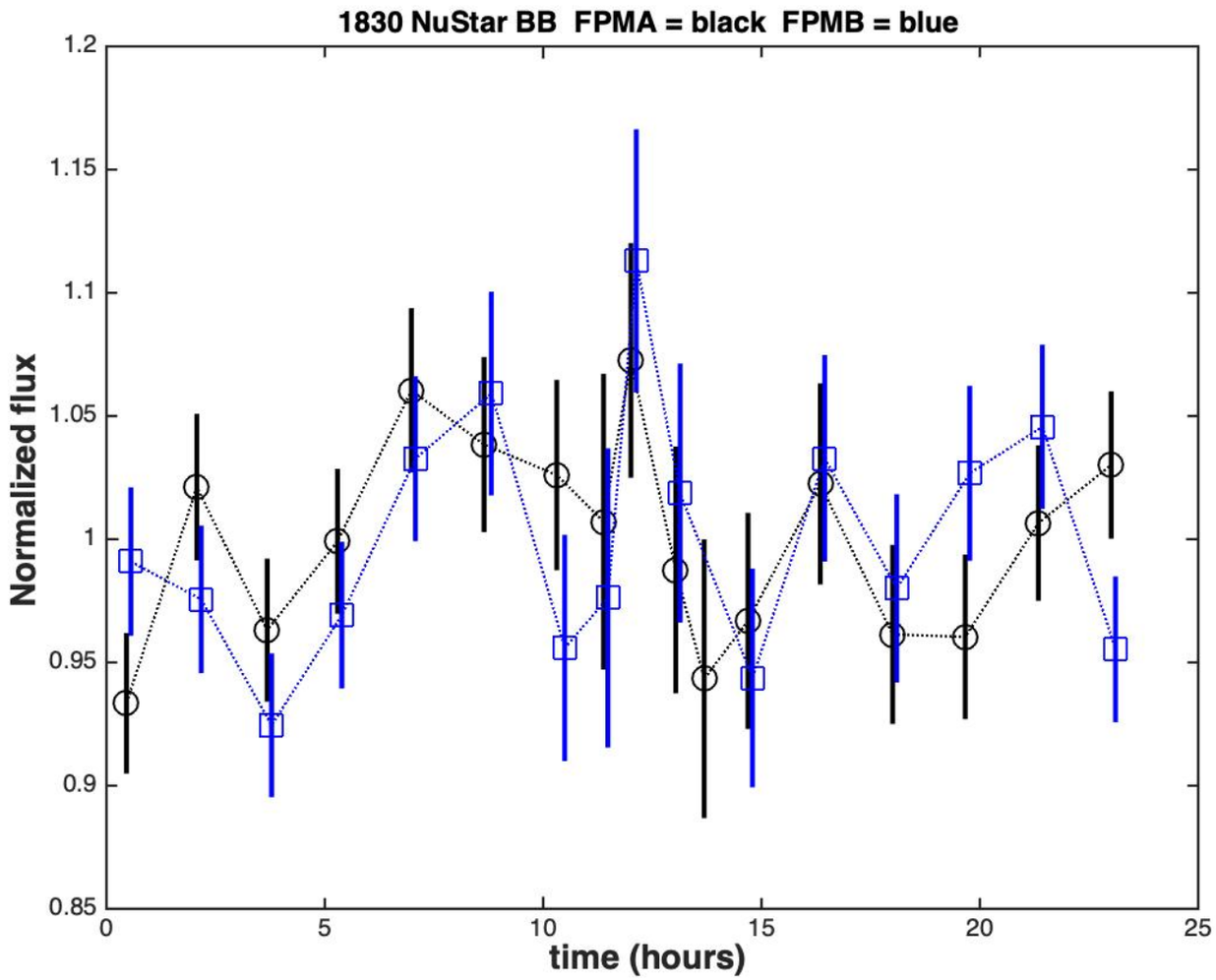

X-ray Variability (NuSTAR)

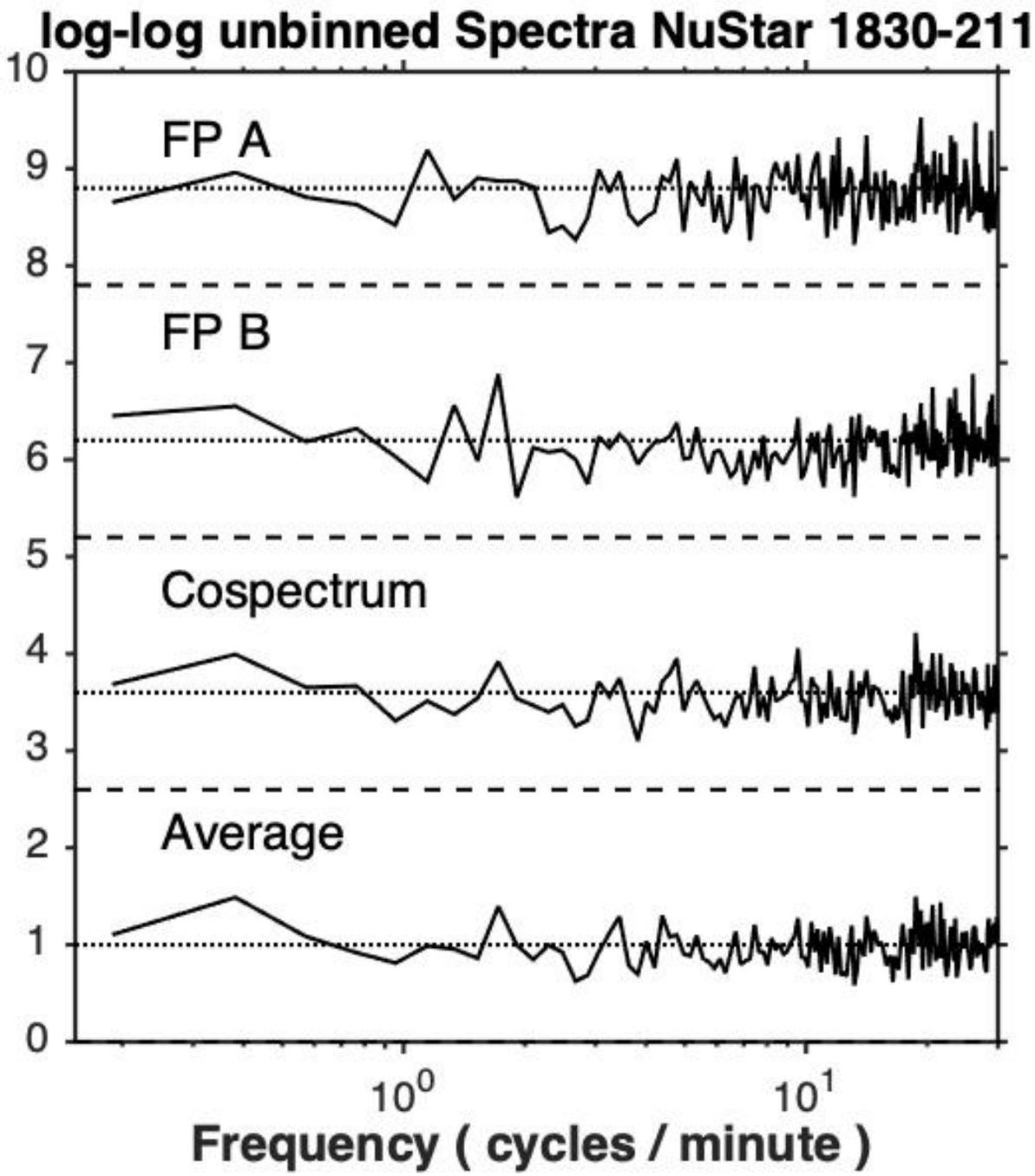

New method: unbinned, time-tagged photon spectrum

- possible for two independent detectors (eg FPMA and FPMB in NuSTAR)
- currently investigating un-binned, time-tagged photon Bayesian block analysis as well

1) tbabs * powerlaw, all fits

in	obsid	n_H	pow-lawi	Cstat	chi	F_(0.5-3	F_(3-10	F_(10-30
S	02	0.66 +/-	1.40 +/- 0.56	19.67 / 10		7.08 e-10		
S	02	0.18	1.02 +/- 0.23	21.26 / 11		4.74 e-10		
N	6016	1.28 +/-	1.488 +/-	499.53 /			1.33 e-11	2.18 e-11
N	6016	0.18	1.447 +/-	503.94 /			1.27 e-11	2.19 e-11
S	16	0.86 +/-	1.18 +/- 0.30	40.34 / 30		5.03 e-12		
S	16	0.18	0.53 +/- 0.13	58.38 / 31		2.73 e-12		
N	02+16+601	1.12 +/-	1.480 +/-	562.45 /		6.79 e-12	1.32 e-11	2.19 e-11
N	02+16+601	0.18	1.406 +/-	746.87 /		4.17 e-12	1.25 e-11	2.26 e-11
S	36	0.73 +/-	1.35 +/- 0.51	4.51 / 12		5.94 e-12		
S	36	0.18	0.90 +/- 0.20	7.22 / 13		3.75 e-12		
N	8046	0.64 +/-	1.458 +/-	718.01 /			1.22 e-11	2.07 e-11
N	8046	0.18	1.440 +/-	719.38 /			1.20 e-11	2.07 e-11
S	37	0.53 +/-	0.98 +/- 0.58	18.89 / 10		4.10 e-12		
S	37	0.18	0.73 +/- 0.23	19.49 / 11		3.19 e-12		
N	36+37+804	0.92 +/-	1.467 +/-	745.32 /		6.59 e-12	1.23 e-11	2.07 e-11
N	36+37+804	0.18	1.432 +/-	790.65 /		4.74 e-12	1.19 e-11	2.08 e-11

Multi-wavelength SED modeling

			BLR_hi			DT_hi		DT_lo	
pc / cm		3,086E+18							
			Model 1	**Model 1a**	**Model 2**	**Model 2a**	**Model 3**	**Model 4**	**Model 5**
magnification	mu		1	10	1	10	10	10	10
distance	r [pc]		0,084	0,084	3,338	3,338	0,324	3,338	0,528
dominant soft photons			BEL	BEL	IR	IR	BEL	IR	IR (*)
Lorentz factor	Gamma		30	30	30	30	20	30	30
jet half-opening angle	theta_j		0,0333	0,0333	0,0333	0,0333	0,05	0,0333	0,0333
viewing angle	theta_obs		0,0333	0,0333	0,0333	0,0333	0,05	0,0333	0,0333
magnetic field	B [G]		0,7	2,25	0,017	0,037	0,093	0,037	0,027
electron energy distribution	gamma_min		1	1	1	1	3	1	1
	gamma_br		580	580	900	900	320	115	300
	gamma_max		1,0E+4	1,0E+4	1,5E+4	1,5E+4	1,0E+4	1,5E+4	1,5E+4
	p_1		1,85	1,85	1,9	1,9	1,9	1,9	1,9
	p_2		3,3	3,2	3,3	3,3	3,1	3,1	3,3
electron jet power	log10 L_e [erg/s]		46,4	45,4	47,4	46,4	46,5	46,2	46,9
proton jet power (no pairs)	log10 L_p [erg/s]		48,9	47,9	49,7	48,7	48,5	48,7	49,3
magnetic jet power	log10 L_B [erg/s]		44,1	45,1	44,1	44,7	43,5	44,7	42,9
radiation jet power	log10 L_r [erg/s]		46,4	45,4	46,5	45,5	45,8	45,0	45,5
fits X-rays			no	no	yes	yes	no	yes	yes

Reference	Delay [d]	Magn.	Range	Data (binning)	Method
van Ommen et al. (1995)	44 ± 9	1.31±0.02	1990 Jun - 1991 Jul	VLA at 8 and 15 GHz	Assume lensed images each consist of core, knot and contribution from Einstein-ring. Determine flux ratio between those components to derive time delay and magnification ratio.
Lovell et al. (1998)	26^{+4}_{-5}	1.52±0.05	1997 Jan - 1998 Jul	ATCA at 8.6 GHz	Dispersion analysis method with flux density light curve of compact component observed in each image.
Wiklind & Combes (2001)	24^{+5}_{-4}	not stated	1996 - 2001	SEST 15 m telescope	Dispersion analysis method with flux of compact component in each image estimated through molecular absorption features.
Barnacka et al. (2011)	27.1 ± 0.6	magn	2008 Aug 4 - 2010 Oct 13	*Fermi*-LAT (2d, 1d, 23h)	double power spectrum
Abdo et al. (2015)	none	magn	2008 Aug 4 - 2011 Jul 25	*Fermi*-LAT (2d, 7d)	auto-correlation
	none	magn	2010 Oct 2 - 2011 Mar 1	*Fermi*-LAT (12h)	(a) auto-correlation: peak at (19 ± 1) d (b) continuous wavelet transform: no well-resolved peak
Barnacka et al. (2015)	23 ± 0.5	magn	2010 Aug 12 - 2011 Feb 28	*Fermi*-LAT (1d)	divided 7d binned LC into 4 flares and used (a) auto-correlation (b) double power spectrum (c) maximum peak ⇒ delay depends on range of LC!
	19.7 ± 1.2	magn	2012 May 3 - 2012 Sep 30		
	none	magn	≈ 2014 Jul 28		
	none	magn	≈ 2015 Jan 8		
Neronov et al. (2015)	21^{+4}_{-5} & 76^{+25}_{-15}	3.1 ± 0.5	2008 Aug - 2014 Sept	*Fermi*-LAT (2d)	structure function and reproduction of Abdo et al. (2015) as well as Lovell et al. (1998)
Abhir et al. (2021)	none	magn	2018 Oct 9 - 2019 Nov 13	*Fermi*-LAT (6h, 12h, 1d, 5d)	auto-correlation (peaks in DCF by eye)

Discrete Correlation Function

$$UDCF_{i,j} = a_i b_j$$

divide in constant bins $\Delta\tau$

according to time shift $\Delta t_{i,j} = t_j - t_i$

Auto-correlation of PKS 1830-211 with LC-binning: 1day